Bistability and hysteresis in an optically injected two-section semiconductor laser

A. Pimenov,[1,*] E. A. Viktorov,[2,3] S. P. Hegarty,[4,5] T. Habruseva,[4,5,6] G. Huyet,[2,4,5] D. Rachinskii,[7,8] and A. G. Vladimirov[1]

[1]*Weierstrass Institute, Mohrenstrasse 39, D-10117 Berlin, Germany*

[2]*National Research University of Information Technologies, Mechanics and Optics, St. Petersburg, Russia*

[3]*Optique Nonlineaire Theorique, Universite Libre de Bruxelles, Campus Plaine, Code Postal 231, B-1050 Bruxelles, Belgium*

[4]*Centre for Advanced Photonics and Process Analysis, Cork Institute of Technology, Cork, Ireland*

[5]*Tyndall National Institute, University College Cork, Lee Maltings, Dyke Parade, Cork, Ireland*

[6]*Aston University, Aston Triangle, B4 7ET Birmingham, United Kingdom*

[7]*Department of Mathematical Sciences, University of Texas at Dallas, Richardson, Texas 75080, USA*

[8]*Department of Applied Mathematics, University College Cork, Cork, Ireland*

(Received 22 January 2014; revised manuscript received 12 April 2014; published 8 May 2014)

The effect of coherent single frequency injection on two-section semiconductor lasers is studied numerically using a model based on a set of delay differential equations. The existence of bistability between different continuous-wave and nonstationary regimes of operation is demonstrated in the case of sufficiently large linewidth enhancement factors.

DOI: 10.1103/PhysRevE.89.052903 PACS number(s): 05.45.−a, 42.55.Px, 42.60.Fc, 42.65.Pc

I. INTRODUCTION

Multisection semiconductor lasers have drawn sustained research interest for their utility in technological applications and as an experimental vehicle for the exploration of nonlinear dynamics concepts. Material growth and device fabrication of semiconductor devices have matured rapidly, offering predictable and quantifiable material and device properties, even over wide operating parameter ranges. An important subcategory is that of two-section, mode-locked semiconductor lasers (MLLs), desired for their ability to generate better than picosecond optical pulses [1], with repetition rates reported from gigahertz to terahertz. Recently, a detailed experimental study has been carried out on two-section quantum-dot MLLs with optical injection. This study reported hysteresis between multiple regimes of operation such as stable mode locking, modulated mode locking, and single-mode lasing. This finding has implications for schemes aimed at improving laser coherence through optical injection, while also opening possibilities for exploiting these bistabilities as optical switches.

As a basic element for optical switches, bistable semiconductor lasers (SLs) have been intensively studied for decades. Optically injected SLs demonstrate multiple effects of bistability and hysteresis for both single-mode [2,3] and multimode devices [4]. Switches in optically injected multimode lasers have been investigated in [5]. Bistability and hysteresis in mode-locked lasers have also been reported in active feedback lasers, where the feedback is amplified in the external cavity [6].

In this paper, we numerically investigate the dynamical states of multisection devices under optical injection from a cw source. Using a traveling wave, ring-cavity model that has been successfully applied to several semiconductor laser types, we identify the appearance of bistabilities and hysteresis between the locked states. Since the origin of hysteresis in these devices has not been studied theoretically so far, our study is mainly focused on the analysis of hysteresis between the simplest single-mode operation regimes of the optically injected laser. We show that asymmetry in the phase-amplitude coupling in the gain and absorber sections is a fundamental requirement for the observation of hysteresis, as experimentally reported for optically injected quantum-dot (QD) lasers [7]. Moreover, by fitting the parameters of the system using experimentally measured pulse profiles, we demonstrate that the observed strong pulse chirp may be related to the large areas of hysteresis between different locked regimes in the parameter plane of injection strength and frequency detuning.

II. MODEL EQUATIONS

A schematic representation of a two-section laser subject to external injection from a single-mode master laser is given in Fig. 1(a). The modeling of two-section lasers can be greatly simplified by treating the laser as a ring cavity. Experimentally, optical injection of two-section mode-locked lasers [7] is typically from the gain section side, and thus amplified by this section before entering the absorber section. To account for this amplification, we consider the ring laser configuration shown in Fig. 1(b), where the gain section is split into two equal parts. The injected external signal first passes through a gain section, then through the absorber section, and, finally, through the second gain section.

Extending the approach developed in [8–10] for two-section mode-locked devices, we describe the laser configuration in Fig. 1(b) by a set of delay differential equations (DDEs):

$$\gamma^{-1}\partial_t A(t) + A(t) = \sqrt{\kappa}\exp\{(1-i\alpha_g)[G_1(t-T) + G_2(t-T)]/2 - (1-i\alpha_q) \times Q(t-T)/2\}A(t-T) + \eta\exp(2\pi i\nu t), \quad (1)$$

$$\tau_g\partial_t G_1(t) = g_0/2 - G_1(t) - (e^{G_1(t)}-1)\,|A(t)|^2, \quad (2)$$

$$\tau_g\partial_t G_2(t) = g_0/2 - G_2(t) - e^{G_1(t)-Q(t)} \times (e^{G_2(t)}-1)\,|A(t)|^2, \quad (3)$$

$$\tau_q\partial_t Q(t) = q_0 - Q(t) - s(1-e^{-Q(t)})e^{G_1(t)}\,|A(t)|^2, \quad (4)$$

*Corresponding author: pimenov@wias-berlin.de

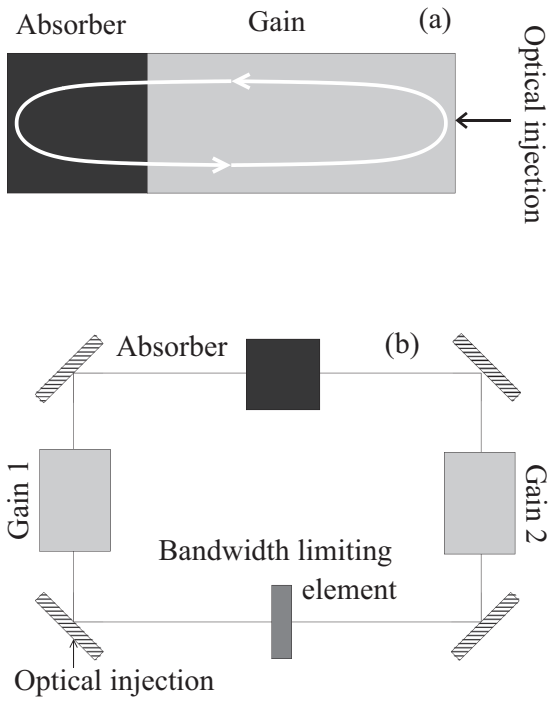

FIG. 1. (a) Schematic representation of an optically injected two-section mode-locked laser. (b) Ring-cavity model of an injected mode-locked laser.

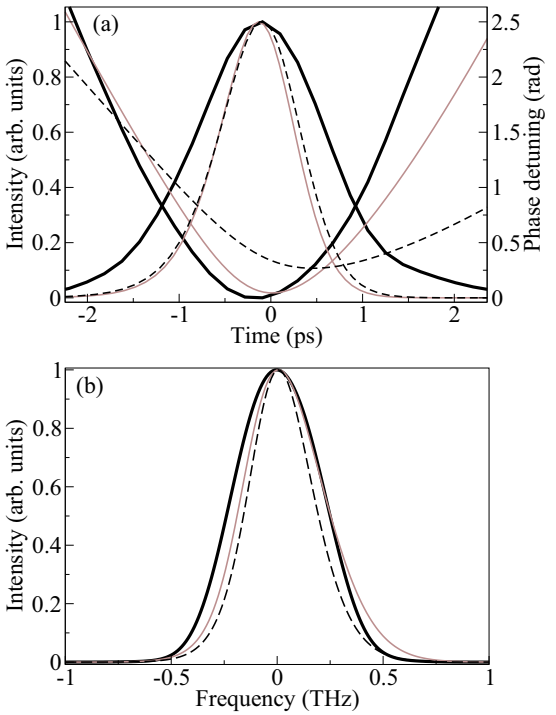

FIG. 2. (Color online) (a) Pulse shapes and phase profiles calculated numerically (thin lines) and measured experimentally (thick lines), where the pulse intensity is normalized to the maximal pulse intensity. The parameter values used in the numerical simulations are $T = 95.864$ ps, $\tau_g = 500$ ps, $\tau_q = 10$ ps, $g_0 = 3.15$, $q_0 = 1.8$, $\kappa = 0.3$, $\gamma = 10$ ps^{-1}, $s = 10$, and $\eta \equiv 0$. Thin solid (dashed) lines correspond to $\alpha_q = 3.5$ and $\alpha_g = 13$ ($\alpha_q = 0.7$ and $\alpha_g = 2$). (b) Mode-locked pulse spectrum calculated numerically (thin lines) and measured experimentally (thick line). Solid (dashed) line corresponds to $\alpha_q = 3.5$ and $\alpha_g = 13$ ($\alpha_q = 0.7$ and $\alpha_g = 2$).

where ∂_t denotes the time derivative and the delay parameter T equals the cold cavity roundtrip time. In Eqs. (1)–(4), $A(t)$ is the normalized complex envelope of the electromagnetic field at the entrance of the first part of the gain section, $G_1(t)$ and $G_2(t)$ describe saturable gain introduced by the two gain sections, and $Q(t)$ is the saturable absorption introduced by the absorber section. The bandwidth of the spectral filtering is γ and the linewidth enhancement factor in the gain (absorber) section is $\alpha_g(\alpha_q)$. $\tau_g = 500$ ps and $\tau_q = 10$ ps are the relaxation times of the gain and absorber sections, respectively, and are broadly representative of semiconductor lasers. $s = 10$ is the typical ratio of the saturation intensities of the gain and absorption. The attenuation factor $\kappa = 0.3$ describes the total nonresonant linear intensity losses per cavity roundtrip. The dimensionless parameters $g_0 = 3.15$ and $q_0 = 1.8$ describe linear unsaturated gain in the gain sections and linear unsaturated absorption in the absorber section, respectively. With these parameters, in the absence of external injection, the laser operates in a mode-locking regime with a pulse repetition rate close to 10 GHz ($T = 95.864$ ps). In the calculations, we use the time variable t/τ_q and dimensionless parameters $T/\tau_q = 9.5864$, and $\tau_g/\tau_q = 50$ normalized to the carrier relaxation time in the absorber section.

The normalized injection rate η and the detuning $\nu = \nu_{\text{inj}} - \nu_{\text{ref}}$ of the master laser signal ν_{inj} from some reference frequency ν_{ref} characterize the coherent optical injection. The reference frequency is set to zero at the maximum gain mode for $\alpha_g = \alpha_q = 0$.

Experimentally measured pulse shape, pulse phase profile, and optical spectrum of a mode-locked regime in a free-running laser ($\eta \equiv 0$) are presented in Fig. 2 by thick lines along with the numerically calculated ones shown by thin lines [7]. In the simulations, all of the parameters of Eqs. (1)–(4) were fixed except for the fitting parameters Γ, α_g, and α_q. The parameters Γ and α_g were used to fit the time and spectral widths of the pulse as well as the pulse phase shift, whereas the parameter α_q allowed us to control the shape of the phase profile. In Fig. 2(a), solid and dashed lines correspond to larger linewidth enhancement factors ($\alpha_g = 13$ and $\alpha_q = 3.5$) and smaller linewidth enhancement factors ($\alpha = 2$ and $\alpha_q = 0.7$), respectively. It is seen from the figure that an increase of the linewidth enhancement factors describing the phase-amplitude coupling in the gain and absorber sections leads to an increase of the pulse chirp and optical spectrum width [11]. The experimental pulse chirp and other pulse characteristics are, thus, reasonably well reproduced by the DDE model (1)–(4) with large difference between linewidth enhancement factors $\alpha_g - \alpha_q$. When the difference $\alpha_g - \alpha_q$ becomes sufficiently large, the mode-locked regime can be destroyed by a transition to quasiperiodic or irregular pulsations [8,11].

III. DYNAMICAL STATES

With the inclusion of optical injection in our simulations, a number of distinct dynamical states become apparent. The different regimes could be distinguished in the numerical simulations by computing the optical spectrum of the laser

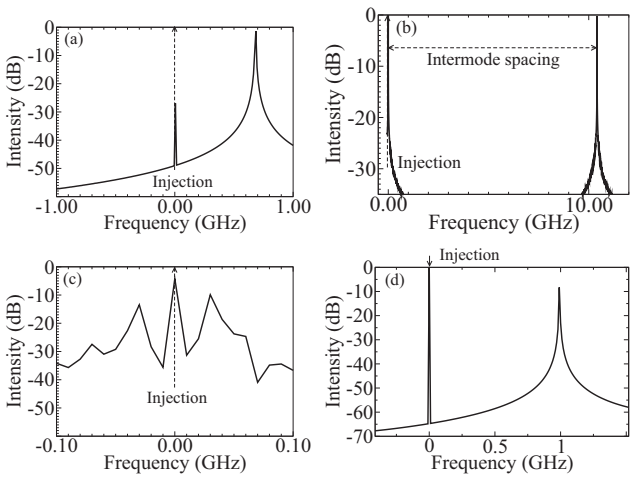

FIG. 3. Optical spectra of injected two-section laser. Enlarged vicinity of the injection frequency in logarithmic scale. $\eta = -40$ dB. (a) U: unlocked regime, $\nu = -46.1549$ GHz. The beating between the laser modes and the injected field can be seen at a distance of 1/10 of the intermode spacing from the injection frequency. (b) ML: locked. The mode-locking tone is similar to U, but no beat tone exists, $\nu = -45.4387$ GHz. (c) LM: locked modulated regime, $\nu = -45.515$ GHz. (d) P: periodically modulated single mode, $\nu = -45.4386$ GHz, $\eta = -17.4598$ dB.

intensity. Representative optical spectra and time traces are displayed in Figs. 3 and 4, correspondingly. We identify five different regimes of operation as follows.

U: unlocked. In this regime, the impact of the injection upon the laser operation was inconsequential, with a weak beat tone developed between the injected light and the adjacent laser modes. The mode-locking frequency is the dominant feature of the power spectrum.

ML: locked. Here, the laser remains mode locked, with one of the laser modes phase locked to the optical injection field. The beat tone between the injected field and the adjacent modes has disappeared and the mode-locking frequency is the only feature of the power spectrum.

LM: locked modulated. In this regime, one laser mode is phase locked to the injection field, but the mode-locking operation is no longer purely periodic, with the emergence of broad sidebands in the optical spectrum.

P: periodic modulation. In this regime, the laser operates in single mode and the mode locking is completely suppressed. The laser intensity is periodically modulated at a frequency substantially less than the mode-locking frequency.

S: single mode. In this regime, the laser operates with a single, unmodulated mode.

The great variety of operating regions in our system suggests using multiple control parameters, which can be collected into three groups. The frequency interval in which locking takes place will be referred to as the locking range, where the normalized injection rate η controls the size of the locking range, as in other optical injection problems. The linewidth enhancement factors α_g and α_q affect the symmetry of the locking boundaries and control the appearance of hysteresis. Finally, we use the spectral filtering bandwidth γ as a suitable control parameter to characterize the hysteresis area, and to confirm the relevance of the scaling law for hysteresis in our multidimensional system.

Figure 5 shows how these regimes are organized in the ν-η plane. The major domains are mapped and labeled using the key given above. These domains were obtained by numerical integration of Eqs. (1)–(4) with rather small linewidth enhancement factors, $\alpha_g = 2$ and $\alpha_q = 0.7$, using the following procedure: For a given injection rate, the injection detuning ν was first increased stepwise from $\nu = -55$ to $\nu = -25$ GHz and then decreased from $\nu = -25$ back to $\nu = -55$ GHz. For each value of ν, the solution calculated at the previous ν value was taken as an initial condition. It is seen from Fig. 5 that each laser mode gives rise to a separate "locking tongue," i.e., a narrow wedge-shaped area where the frequency of this mode can be locked to the frequency of the external injection ν (black and dark gray areas). The results presented in Fig. 5 are in qualitative agreement with the results of experimental measurements at low injection powers [7] and show no bistability between the different regimes of operation.

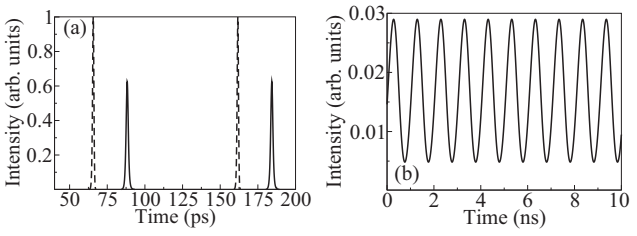

FIG. 4. Time traces of the regimes, whose spectra are plotted in Fig. 3. (a) ML: locked; dashed line: intensity of the free-running laser, $\eta \equiv 0$, normalized to 1; solid line: $\nu = -45.515$ GHz, $\eta = -40$ dB. In the locked regime (ML), the number of locked modes is usually smaller than in the free-running passively mode-locked laser, and, hence, the pulse width is larger. (b) P: periodically modulated single mode, $\nu = -45.4386$ GHz, $\eta = -17.4598$ dB. The LM and U regimes look similar to (a), but with slow low-intensity modulation.

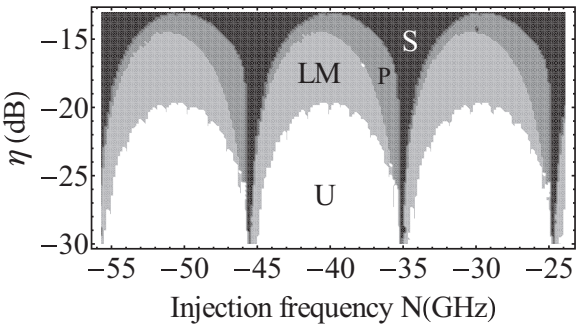

FIG. 5. Different dynamical regimes calculated numerically for small values of the linewidth enhancement factors, $\alpha_g = 2$ and $\alpha_q = 0.7$. In white areas (U), the laser is not locked to the external signal. White areas (U) correspond to the mode-locking regimes very slightly affected by the external injection, while in light gray areas (LM), the laser is in locked modulated multimode regime. The dark gray areas (P) correspond to periodic single-mode regimes with laser output intensity oscillating periodically at a frequency much smaller than the intermode frequency separation. cw regimes are indicated by a black color (area S).

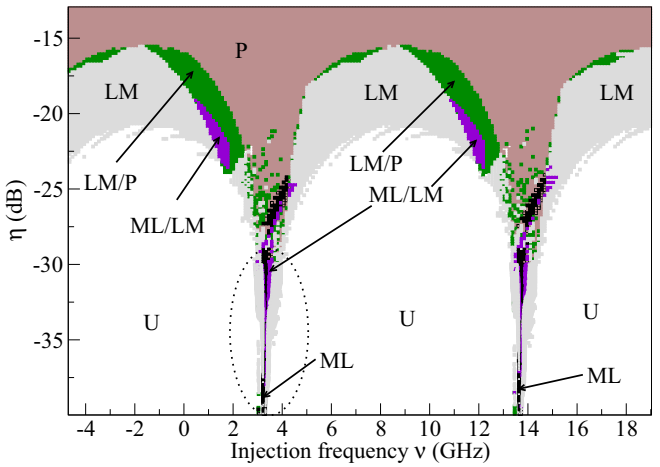

FIG. 6. (Color online) Domains of different operation regimes calculated numerically for $\alpha_g = 13$ and $\alpha_q = 3.5$. Area P corresponds to time-periodic single-mode regimes locked to the injection frequency, black areas ML correspond to mode-locked regimes synchronized to the injection frequency, and areas LM correspond to multimode regimes with modulated laser intensity. Other colored areas show bistability domains between different operation regimes: LM/P: modulated/periodic; ML/LM: mode locked/modulated.

The maps presented in Figs. 6 and 7 are similar to that shown in Fig. 5, but correspond to larger values of the linewidth enhancement factors in the gain and absorber sections, $\alpha_g = 13$ and $\alpha_q = 3.5$. It is seen that at large injection rate, instead of cw regimes indicated by the letter S in Fig. 5, we have periodically modulated single-mode regimes; see area P in Fig. 6. For the values of linewidth enhancement factors corresponding to Fig. 6, cw regimes appear at much higher injection rates ($\eta > -13$ dB) than for the parameter values of Fig. 5, therefore, these regimes are not shown in Fig. 6. Figure 7 presents an enlarged view of the area encircled by the dashed line in Fig. 6. In these two figures in the domain indicated by ML/LM, the laser exhibits a bistability between the locked modulated multimode

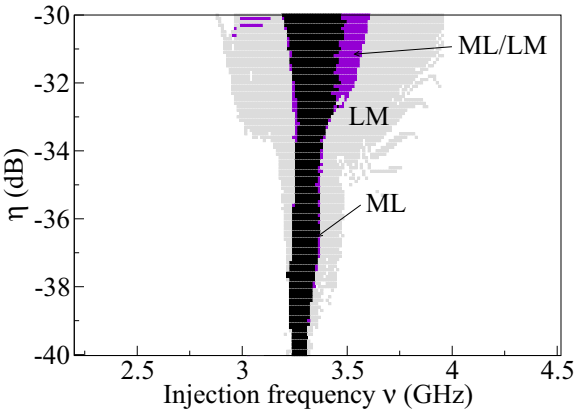

FIG. 7. (Color online) Zoom of one of the locking tongues shown in Fig. 6 at small injection rate. Bistability domains between locked modulated and mode-locked solutions are indicated as ML/LM. Black area ML corresponds to the domain of mode-locking regimes locked to the injection frequency.

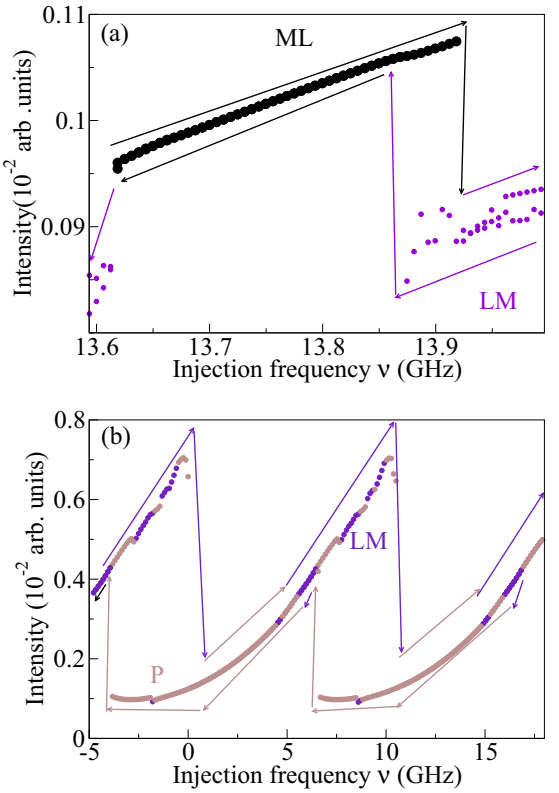

FIG. 8. (Color online) Bistability between different laser operation regimes. Arrows indicate the direction in which the frequency detuning ν is changed. (a) $\eta = -32.2185$ dB. Small circles represent the locked modulated multimode regime; big circles represent the mode-locked regime. When the detuning is increased, the transition from mode-locked regime (big circles) to locked modulated regime (small circles) occurs at $\nu \approx 13.92$ GHz, whereas when the detuning is decreased, the opposite transition from locked modulated regime to mode-locked regime takes place at $\nu \approx 13.87$ GHz. (b) $\eta = -13.9794$ dB. Dark points: locked modulated regimes; light points: periodic regimes. When the detuning is decreased, a transition from periodic regime to locked modulated regime occurs at $\nu \approx 6$ GHz, whereas when the detuning is increased, the opposite transition takes place at $\nu \approx 10$ GHz.

and mode-locked regimes. Furthermore, in the areas labeled LM/P in Fig. 6, single-mode periodically modulated regimes are bistable with locked modulated multimode ones. The corresponding branches of solutions are presented in Fig. 8. The cusp catastrophe induced bistability is normally expected in a system with strong asymmetry. Such an asymmetry in the two-section device can be attributed to sufficiently different strength of the phase-amplitude coupling in the gain and absorber section. We find that a significant difference between α_g and α_q is a necessary condition for bistable operation in our system. Moreover, we show that the strong phase-amplitude coupling induced by the large difference between linewidth enhancement factors (see Fig. 2) leads to wide areas of hysteresis between different regimes (see Fig. 6). Both the strong pulse chirp (see Fig. 2) and the large regions of bistability were observed in the experiment [7] as well, which may indicate that these two phenomena are directly related. We note, however, that the in-depth analysis of the mechanism

responsible for the strong amplitude-phase coupling in QD devices is far beyond the scope of this work. Furthermore, although our theoretical analysis was successful in identifying all the regimes and bistability domains reported in [7], direct comparison of Fig. 6 with the experimental diagram reveals significant differences in the location of the bistability domains inside the locking tongues as well as geometrical shapes of the boundaries of these domains. These differences cannot be explained using the model equations (1)–(4), which do not take into account specific features of QD materials.

IV. HYSTERESIS

We have analyzed the bifurcations leading to bistability of cw and periodically modulated single-mode regimes at high injection rates beyond the range shown in Fig. 5. In order to perform the analysis, we have used the path-following software package DDE-BIFTOOL [12]. In order to apply this package to the system (1)–(4), we transform it into an autonomous set of equations by shifting the frequency reference $A \to Ae^{2\pi i\nu t}$. The branch of single-mode solutions obtained by changing the injection detuning parameter ν is shown in Fig. 9(a). It is seen that when the detuning ν is changed, the laser intensity oscillates almost periodically on this branch with a period close to the free spectral range $1/T$. Each oscillation period of the branch contains two segments corresponding to a stable cw solution: one of them bounded by a fold bifurcation point A from the right side and by an Andronov-Hopf bifurcation point D from the left side, and the other one bounded by an Andronov-Hopf bifurcation point C from the right side and by a fold point B from the left side. These segments are indicated by solid black lines. Between points D and C, the branch of cw solutions is unstable with respect to a self-pulsing instability (dashed line). It is seen from Fig. 9(a) that there is a bistability between cw and periodically modulated single-mode solutions within certain frequency ranges. The origin of this bistability can be understood by noticing that a part of the cw branch BCDAB demonstrates a typical example of nonlinear resonance behavior with resonant frequency close to the frequency of the corresponding longitudinal laser mode. Due to the multiplicity of the modes, the cw branch exhibits multiple resonances, each corresponding to a certain longitudinal mode of a mode-locked laser. In the case of nonzero linewidth enhancement factors, modal frequencies depend on the injection amplitude. In particular, it is seen from Fig. 9(a) that in the case when $\alpha_g > \alpha_q > 0$, modal frequencies increase with the injection rate η. This dependence of modal frequencies on the injection rate can lead to an overlap of the resonances corresponding to neighboring longitudinal modes and, hence, to the appearance of bistability and hysteresis. Therefore, experimental observations of bistability and hysteresis in an optically injected QD mode-locked laser [7] are consistent with the earlier experiments, indicating that the α factor in the QD based semiconductor gain noticeably increases above threshold [13,14], and also with the theoretical analysis of the present paper. As one can see in Fig. 9(b), the overlap of the resonances corresponding to neighboring longitudinal modes appears between two fold bifurcation points, A and B, when the absolute value of the difference of the two linewidth enhancement factors $|\alpha_g - \alpha_q|$

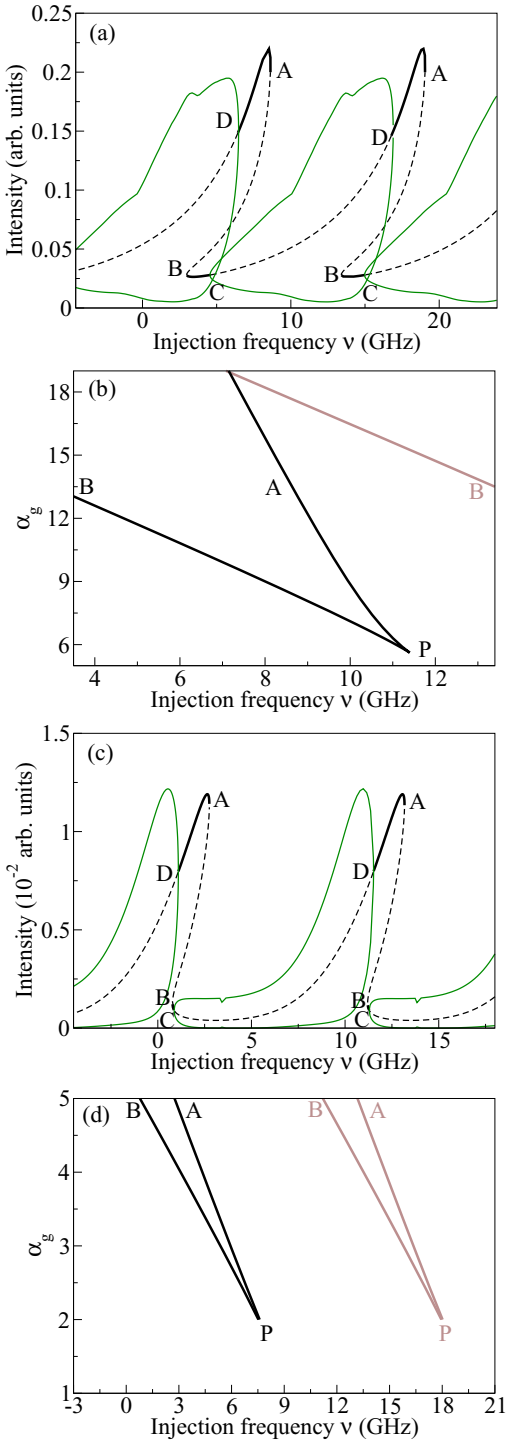

FIG. 9. (Color online) Bifurcation diagrams for Eqs. (1)–(4) obtained numerically using the software package DDE-BIFTOOL. The injection is strong, $\eta = -6.0206$ dB. Other parameters are the same as in Fig. 6. (a) Branches of cw and periodically modulated single-mode solutions. Stable and unstable parts of the cw branch are shown by black solid thick and dashed lines, respectively. Solid thin lines represent the minima and maxima of solutions with time-periodic intensity. A and B indicate fold bifurcations; C and D indicate Andronov-Hopf bifurcations. (b) Bistability domain is located between two fold bifurcation lines, A and B. P is the codimension-two cusp bifurcation point. (c),(d) The same as (a) and (b), but for $\alpha_q = 0, \alpha_g = 5$, and $\eta = -13.9794$ dB.

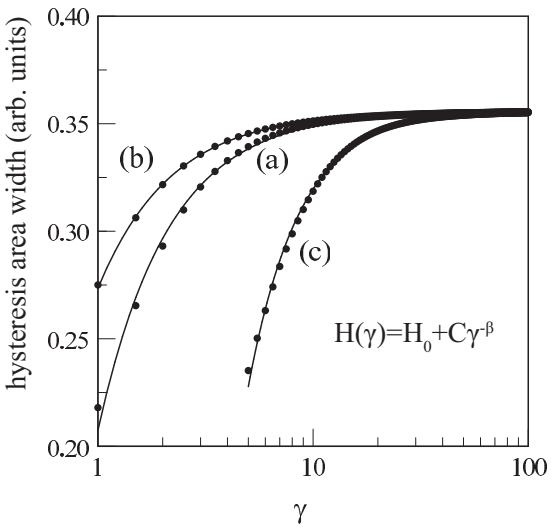

FIG. 10. Numerical results (dots) and corresponding fits (solid lines) for the width of the hysteresis area in Figs. 9(a) and 9(b) as a function of the bandwidth γ, which is calculated as the distance between the points A and B along the ν axis. The scaling exponent β is 1.3 for (a) $\nu = 0$ and (b) 15 GHz, and 1.8 for (c) $\nu = 95$ GHz.

is sufficiently large. With the decrease of the linewidth enhancement factor α_g in the gain section, the two fold bifurcations corresponding to lines A and B come closer and closer to one another and, finally, merge and annihilate at the cusp bifurcation point P. Below this point, there is no bistability and hysteresis in the model. The presence of bistability at sufficiently large linewidth enhancement factors assumes abrupt jumps between the solutions corresponding to neighboring longitudinal modes. Similar jumps between cw and periodically modulated single-mode regimes were observed experimentally and demonstrated theoretically in a multimode semiconductor laser without a saturable absorber section [5].

The cusp hysteresis has been observed in numerous dynamical systems, and possesses some universal scaling laws for hysteresis loop area (width). In order to characterize the cusp hysteresis in Figs. 9(a) and 9(b), we chose the filter bandwidth γ as a control parameter. The bifurcation diagram in Figs. 9(a) and 9(b) remains largely unchanged for a broad range of γ, which allows appropriate calculation of the hysteresis width as a function of the control parameter. The results are shown in Fig. 10 for different values of the detuning ν. The hysteresis width $H(\gamma)$ is given by $H(\gamma) = H_0 + C\gamma^{-\beta}$. The scaling exponent β remains the same for a small variation of ν around the optical spectrum peak ($\nu = 0$ and 15 GHz), but increases for injection closer to the side modes away from the peak ($\nu = 95$ GHz). It indicates that the weaker side modes are more sensitive to the injection with a faster change of the hysteresis area.

Finally, to illustrate the effect of the linewidth enhancement factors on the size of the hysteresis loop, we replot Figs. 9(a) and 9(b) with smaller linewidth enhancement factors, $\alpha_q = 0$ and $\alpha_g = 5$. The result is shown in Figs. 9(c) and 9(d), where the bistability can exist at rather moderate values of the linewidth enhancement factors in the gain section, $\alpha_g \geqslant 2$. From our simulations, we conclude that the width of the hysteresis loop depends mainly on the difference $|\alpha_g - \alpha_q|$.

V. CONCLUSION

To conclude, using a modification of the delay differential mode-locking model proposed in [8–10], we have performed a numerical study of the operation regimes of an optically injected semiconductor mode-locked laser. We have shown that similarly to reported experimental results [7,15], bistability and hysteresis can exist between different laser operation regimes. This bistability appears for sufficiently large difference between the linewidth enhancement factors in the gain and absorber sections and is related to overlapping nonlinear resonances corresponding to different longitudinal laser modes. When the difference between linewidth enhancement factors is sufficiently small, there is no bistability in the model equations.

ACKNOWLEDGMENTS

A.P. and A.G.V. acknowledge the support of SFB 787 of the DFG, Project No. B5. T.H. acknowledges the support of Marie Curie Action FP7-PEOPLE-2011-IEF, HARMOFIRE project, Grant No. 299288. G.H., S.P.H., and A.G.V. acknowledge the support of EU FP7 Marie Curie Action FP7-PEOPLE-2010-ITN through the PROPHET project, Grant No. 264687. A.G.V. and G.H. acknowledge the support of E. T. S. Walton Visitors Award of the SFI. G.H. and S.P.H. were also supported by the Science Foundation Ireland (SFI) under Contract No. 11/PI/1152, and under the framework of the INSPIRE Structured Ph.D. Programme, funded by the Irish Government's Programme for Research in Third Level Institutions, Cycle 5, National Development Plan 2007–2013.

[1] E. U. Rafailov, M. A. Cataluna, and W. Sibbett, Nat. Photon. **1**, 395 (2007).
[2] T. Erneux, E. A. Viktorov, B. Kelleher, D. Goulding, S. P. Hegarty, and G. Huyet, Opt. Lett. **35**, 937 (2010).
[3] A. Hohl, H. J. C. van der Linden, R. Roy, G. Goldsztein, F. Broner, and S. H. Strogatz, Phys. Rev. Lett. **74**, 2220 (1995).
[4] P. Heinricht, B. Wetzel, S. O'Brien, A. Amann, and S. Osborne, Appl. Phys. Lett. **99**, 011104 (2011).
[5] J. K. White, J. V. Moloney, A. Gavrielides, V. Kovanis, A. Hohl, and R. Kalmus, IEEE J. Quantum Electron. **34**, 1469 (1998).
[6] S. Bauer, O. Brox, J. Kreissl, B. Sartorius, M. Radziunas, J. Sieber, H.-J. W. ünsche, and F. Henneberger, Phys. Rev. E **69**, 016206 (2004).
[7] T. Habruseva, S. P. Hegarty, A. G. Vladimirov, A. Pimenov, D. Rachinskii, N. Rebrova, E. A. Viktorov, and G. Huyet, Opt. Express **20**, 25572 (2012).

[8] A. G. Vladimirov and D. Turaev, Phys. Rev. A **72**, 033808 (2005).
[9] A. G. Vladimirov, D. Turaev, and G. Kozyreff, Opt. Lett. **29**, 1221 (2004).
[10] A. G. Vladimirov and D. V. Turaev, Radiophys. Quantum Electron. **47**, 769 (2004).
[11] A. G. Vladimirov, A. S. Pimenov, and D. Rachinskii, IEEE J. Quantum Electron. **45**, 462 (2009).
[12] K. Engelborghs, T. Luzyanina, and D. Roose, ACM Trans. Math. Software **28**, 1 (2002).
[13] T. Piwonski *et al.*, J. Appl. Phys. **106**, 083104 (2009).
[14] B. Dagens, A. Markus, J. X. Chen, J.-G. Provost, D. Make, O. Le Gouezigou, J. Landreau, A. Fiore, and B. Thedrez, Electr. Lett. **41**, 323 (2005).
[15] A. Hurtado, M. Nami, I. D. Henning, M. J. Adams, and L. F. Lester, Appl. Phys. Lett. **101**, 161117 (2012).